GEOCHEMISTRY

Sedimentary sulfur isotopes and Neoarchean ocean oxygenation

Mojtaba Fakhraee,[1]* Sean A. Crowe,[2] Sergei Katsev[1,3]*

Abrupt disappearance of mass-independent fractionation of sulfur isotopes (MIF-S) from the geologic record and an apparent ingrowth in seawater sulfate around 2.45 billion years ago (Ga) signal the first large-scale oxygenation of the atmosphere [the Great Oxygenation Event (GOE)]. Pre-GOE O_2 production is evident from multiple other terrestrial and marine proxies, but oceanic O_2 concentrations remain poorly constrained. Furthermore, current interpretations of S isotope records do not explain a concurrent expansion in the range of both MIF-S—diagnostic for low atmospheric O_2—and $\delta^{34}S$ beginning at 2.7 Ga. To address these unknowns, we developed a reaction-transport model to analyze the preservation patterns of sulfur isotopes in Archean sedimentary pyrites, one of the most robust and widely distributed proxies for early Earth biogeochemistry. Our modeling, paradoxically, reveals that micromolar levels of O_2 in seawater enhance the preservation of large MIF-S signals, whereas concomitant ingrowth of sulfate expands the ranges in pyrite $\delta^{34}S$. The 2.7- to 2.45-Ga expansion in both $\Delta^{33}S$ and $\delta^{34}S$ ranges thus argues for a widespread and protracted oxygenation of seawater, at least in shallow marine environments. At the micromolar levels predicted, the surface oceans would support a strong flux of O_2 to the atmosphere, where O_2 sinks balanced these fluxes until the GOE. This microoxic seawater would have provided habitat for early aerobic microorganisms and supported a diversity of new O_2-driven biogeochemical cycles in the Neoarchean.

INTRODUCTION

Two key features of sulfur isotope distributions in Archean pyrites underpin assertions for very low Archean atmospheric O_2 concentrations: records of large mass-independent fractionations of sulfur isotopes ($\Delta^{33}S$; MIF-S) (*1*–*3*) and a narrow range of $\delta^{34}S$ values (*4*). MIFs are produced in an ozone-free atmosphere, and atmospheric photochemical models suggest delivery of MIF-S to the Earth's surface only when atmospheric O_2 concentrations are less than 10^{-5} present atmospheric levels (*1*, *2*). The relatively restricted ranges of $\delta^{34}S$ in Archean pyrites, particularly before 2.7 billion years ago (Ga), point to low sulfate concentrations in the oceans, reflecting both restricted oxidative weathering of pyrites on land and little oxidative recycling of sulfur in the oceans (*5*, *6*). Thus, the broad-scale features of the $\Delta^{33}S$ and $\delta^{34}S$ records paint a coherent picture of Archean atmospheric chemistry—low O_2 concentrations that lead to both extensive photochemical sulfur cycling imparting large MIF and limited biogeochemical sulfur cycling at the Earth's surface imparting small mass-dependent fractionations (MDFs). There is, however, a more nuanced structure to the Archean S isotope record including an expansion in the ranges of both $\Delta^{33}S$ and $\delta^{34}S$ between 2.7 and 2.45 Ga (Fig. 1). The $\Delta^{33}S$ expansion was attributed to changes in the oxidation state of volcanic sulfur vented to the atmosphere (*7*), whereas the $\delta^{34}S$ expansion was thought to reflect increased sulfate concentrations in oceans (*4*). Here, we show that the Neoarchean records of $\Delta^{33}S$ and $\delta^{34}S$ both indicate progressive seawater oxygenation beginning at 2.7 Ga, and our models constrain the corresponding levels of O_2 and sulfate in Archean coastal environments.

RESULTS AND DISCUSSION

The $\delta^{34}S$ and $\Delta^{33}S_{FeS2}$ isotopic records preserved in Archean sedimentary pyrites carry signatures of atmospheric processes as well as information about isotopic alterations taking place in oceanic water column and in sediments after their deposition. The transformations during early diagenesis were investigated here with a one-dimensional reaction-transport model, which traced the differential dynamics of sulfur isotopes through a network of geochemical and biogeochemical reactions (see Methods and the Supplementary Materials) and provided insights into the preservation patterns of S isotopes and the role of oxygen in them.

The pre-GOE (Great Oxygenation Event) expansion in sulfate-pyrite $\delta^{34}S$ isotopic differences, $\varepsilon_{SO4\text{-}FeS2}$, has been previously ascribed to rising seawater sulfate concentrations, which lead to more intense sedimentary sulfate reduction and generate isotopically lighter pyrite (*4*, *8*). Our simulations support this conclusion but additionally suggest that the presence of dissolved O_2 also increases the $\delta^{34}S$ range by intensifying in-sediment sulfate-sulfide redox cycling. Low-micromolar O_2 concentrations, however, only increase $\varepsilon_{SO4\text{-}FeS2}$ by a few per mil, because sulfur cycling remains limited and fractionation during sulfide oxidation is minor in comparison to that imparted during sulfate reduction (Fig. 2A). The effect of O_2 on the preservation of $\Delta^{33}S$ signatures, in contrast, is pronounced. Oxygen in the atmosphere is generally thought to preclude the formation of MIF-S due to ozone formation and the shielding of the ultraviolet radiation needed for SO_2 photolysis (*9*, *10*). Our modeling, on the other hand, reveals that O_2 in the ocean enhances the preservation of MIF-S in pyrite (Fig. 2B). Pyrite is typically formed when iron monosulfide reacts with either elemental S or hydrogen sulfide (R_{FeS+S} and R_{FeS+HS} in table S1). When the atmospheric MIF-S signal is transmitted from elemental S to pyrite through diagenesis, it is thus influenced by the isotopic composition of iron monosulfide and porewater hydrogen sulfide (fig. S1). Because hydrogen sulfide can be produced from non–MIF-S sulfate through microbially catalyzed reactions such as sulfate reduction that impart MDF, its addition to pyrite dilutes the MIF-S signal. Hydrogen sulfide precipitation with ferrous iron generates iron monosulfide, the isotopic composition of which becomes a complex function of the intensity of sulfate reduction, recycling of hydrogen sulfide through redox processes within sediment, and Rayleigh distillation (*11*, *12*). These processes make the MIF-S signatures in pyrite dependent on the rate of sulfate reduction, which is regulated by the availability of

[1]Large Lakes Observatory, University of Minnesota Duluth, 2205 East 5th Street, Duluth, MN 55812, USA. [2]Department of Microbiology and Immunology and Department of Earth, Ocean, and Atmospheric Sciences, University of British Columbia, Vancouver, British Columbia V6T 1Z4, Canada. [3]Department of Physics and Astronomy, University of Minnesota Duluth, Duluth, MN 55812, USA.
*Corresponding author. Email: fakhr008@umn.edu (M.F.); skatsev@d.umn.edu (S.K.)

sulfate and reactive organic matter (*13*), and several other factors involved in sediment S cycling (Figs. 2B and 3 and fig. S6). Oxygen plays a key role by controlling oxidative S cycling and the supply of reactive organic matter available to fuel sulfate reduction. In particular, higher O_2 levels enhance the preservation of MIF-S signals (Fig. 2B) by decreasing the sulfate reduction rates through deepening of the depth of the sulfate reduction zone in the sediment and limiting the supply of reactive organic matter reaching that zone. In contrast to the effect of O_2, increased sulfate levels result in more intense sulfate reduction and hydrogen sulfide production, and more intense dilution of the MIF-S signal, resulting in lower $\Delta^{33}S$ (Figs. 2B and 3 and figs. S6 and S7).

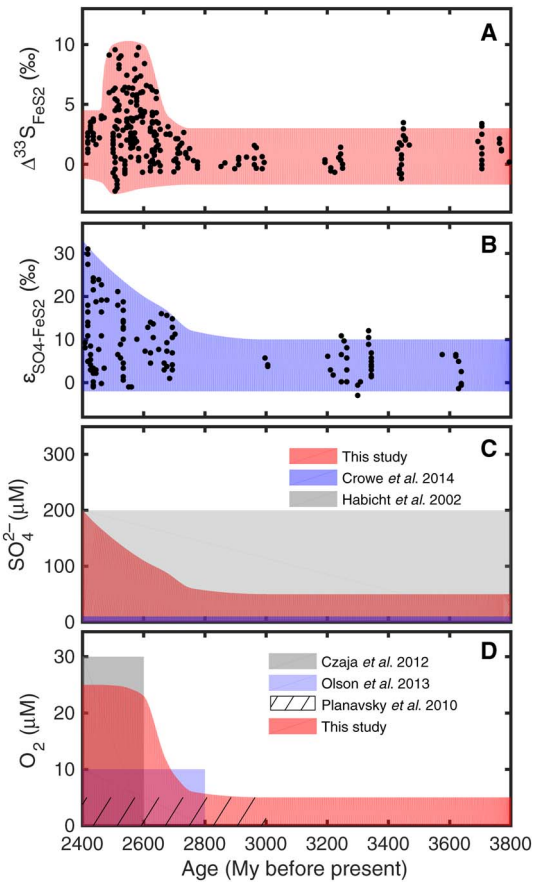

Fig. 1. Changes in $\Delta^{33}S_{FeS2}$, $\varepsilon_{SO4\text{-}FeS2}$, oceanic sulfate, and oxygen throughout the Archean. Record of (**A**) $\Delta^{33}S_{SO4\text{-}FeS2}$ and (**B**) $\varepsilon_{SO4\text{-}FeS2}$ (assuming a seawater sulfate value of 12‰) and the simulated (**C**) oceanic sulfate and (**D**) O_2 levels through time. Data points are from Canfield and Farquhar (*5*) and Johnston (*33*). Simulated outlines for sulfate and O_2 concentrations correspond to values for which our model reproduces the S isotope records. My, million years.

Isotopic variability induced by rising marine O_2 and concomitant increases in seawater sulfate provide a self-consistent explanation for the observed Neoarchean expansions in $\Delta^{33}S$ and $\delta^{34}S$ ranges. In Archean rocks, high values of $\Delta^{33}S$ tend to be associated with low values of $\varepsilon_{SO4\text{-}FeS2}$, whereas larger values of $\varepsilon_{SO4\text{-}FeS2}$ tend to occur at low $\Delta^{33}S$ (Fig. 3). This pattern has been attributed to variability in the atmospheric processes that produce MIF-S (*7*). Figure 3 illustrates that diagenetic processes can impart a similar relationship, where $\delta^{34}S$ and $\Delta^{33}S$ covary depending on seawater O_2 and sulfate concentrations. The increase in $\Delta^{33}S$ variability in the Neoarchean was previously attributed to changes in the oxidation state of volcanic sulfur emitted to the atmosphere (*7*) and to the associated shift in photochemical S transformation pathways (*7*, *14*, *15*). This explanation, however, relies on the assumption that atmospherically produced MIF-S signals remain unmodified by diagenesis (*7*), which requires persistently negligible sediment sulfate reduction. This conflicts with recent evidence for increased microbial sulfate reduction in the Neoarchean (*16*) and with the correlative expansion in $\varepsilon_{SO4\text{-}FeS2}$, which is a known indicator for increased sulfate concentrations and enhanced rates of sulfate reduction (*4*). Furthermore, there remains no known geological process that would induce the inferred shift in the oxidation state of volcanic gases before the GOE. Our model suggests instead that the Neoarchean expansion in $\Delta^{33}S$ and $\delta^{34}S$ reflects the protracted oxygenation of seawater and an early ingrowth in marine sulfate (Fig. 3).

Comparisons of our model results with the $\delta^{34}S$ and $\Delta^{33}S$ compositions of Archean pyrites allow us to constrain the O_2 and sulfate levels of contemporaneous seawater and identify the effects of several diagenetic factors on the preserved sulfur isotopic signatures (Fig. 3). The concentrations of O_2 and sulfate required to reproduce given the $\delta^{34}S$ and $\Delta^{33}S$ ranges depend on factors such as sediment organic matter concentration and the isotopic values of elemental S and sulfate delivered to the sediment (Fig. 3). The narrow mid-Archean ranges of both $\delta^{34}S$ and $\Delta^{33}S$ require pyrite formation under very low O_2 and low sulfate concentrations. The preservation of large values of $\Delta^{33}S$ observed after

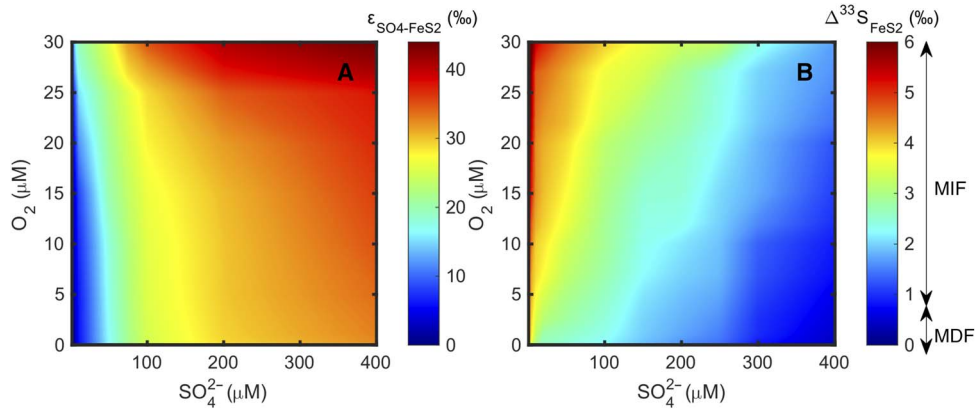

Fig. 2. Modeled range of $\varepsilon_{SO4\text{-}FeS2}$ and $\Delta^{33}S_{FeS2}$ for different oxygen and sulfate concentrations. (**A**) Modeled range of $\delta^{34}S$ isotopic differences between seawater sulfate and sedimentary pyrites ($\varepsilon_{SO4\text{-}FeS2}$) for different O_2 and sulfate levels. (**B**) Modeled range of $\Delta^{33}S_{FeS2}$ for which the atmospheric MIF-S signal is preserved in sedimentary pyrites, as a function of seawater O_2 and sulfate levels. Up-down arrows correspond to the respective ranges of MIF and MDF. Higher-resolution details at the low sulfate range are provided in fig. S6.

2.7 Ga, in contrast, requires a rise in seawater O_2 concentrations to several micromolar. The correlative increase in $\varepsilon_{SO4\text{-}FeS2}$ signals a contemporaneous increase in seawater sulfate to concentrations on the order of 200 μM. Increased sulfate alone, however, does not reproduce the $\varepsilon_{SO4\text{-}FeS2}$ record, which also requires enhanced deposition of OC (Fig. 3) because, even at low sulfate levels, sulfate reduction becomes co-limited by organic substrates (*13*). The Neoarchean S isotope expansion, therefore, likely signals not only the onset of marine oxidative sulfur cycling but also an increase in the ocean's biological productivity, at least in localized coastal oxygen oases.

S isotopes thus paint a cogent picture of Neoarchean ocean oxygenation that is supported by insight from other proxies. Abundant evidence implies O_2 production across more than 700 million years before the GOE (*6*, *17*–*21*). Development of ocean O_2 "oases" at the onset of the Neoarchean era with concentrations up to tens of micromolar is supported by inferences from the geochemistries of molybdenum (*18*) and manganese and iron (*22*, *23*), whereas cerium anomalies in carbonates (*23*) imply shallow water O_2 concentrations approaching ~5 μM O_2. Our model supports these estimates and shows that micromolar O_2 concentrations in the ocean are compatible with (*24*–*27*) and are possibly even required by the MIF-S record. Global biogeochemical models reveal that seawater O_2 concentrations on the order of 1 to 10 μM (*27*), and possibly up to 25 μM, can exist under an ostensibly anoxic atmosphere, despite large fluxes of O_2 from the ocean (*28*). Further, the Neoarchean development of coastal euxina (*6*) may also reflect an accompanying increase in seawater sulfate concentrations resulting from enhanced oxidative continental weathering. Our results further suggest that broadening of the $\delta^{34}S$ range during the GOE, after the disappearance of the MIF-S signal (~2.5 to 2.4 Ga; Fig. 1), reflects an increase in seawater O_2 from low micromolar concentrations to beyond a threshold value of tens of micromolar. The sensitivity of pyritic $\varepsilon_{SO4\text{-}FeS2}$ values to O_2 is dependent on microbial physiology but increases markedly in the range of 10 to 15 μM (see the Supplementary Materials). The approximately 10‰ increase in $\varepsilon_{SO4\text{-}FeS2}$ observed at the GOE thus likely indicates a transition from low micromolar seawater O_2 concentrations to several tens of micromolar, rather than its first production and accumulation.

The Neoarchean era was thus characterized by a major reorganization of the global S cycle that saw an ingrowth of seawater sulfate, the onset of oxidative sediment sulfur cycling, and an increase in the role of sediment sulfate reduction beginning around 2.7 Ga. This reorganization, captured in the isotopic composition of carbonate-associated sulfate (*16*), made microbial sulfate reduction an important sink for marine sulfate (*16*). The onset of O_2-driven marine sulfur cycling, as revealed by the sulfur isotope record (*5*), signals a broader expansion of the oxic marine biosphere and the proliferation of aerobic microbial metabolisms likely linked to heterotrophic carbon respiration and possibly methanotrophy and oxidative nitrogen cycling in the sea.

METHODS

Geochemical and isotopic modeling

Transformations of S from seawater sulfate and MIF-carrying elemental S deposited from the atmosphere were simulated at steady state with a diagenetic equation

$$0 = D_i \varphi \frac{d^2 C_i}{dx^2} - v \frac{dC_i}{dx} + \sum_j R_{ij} \quad (1)$$

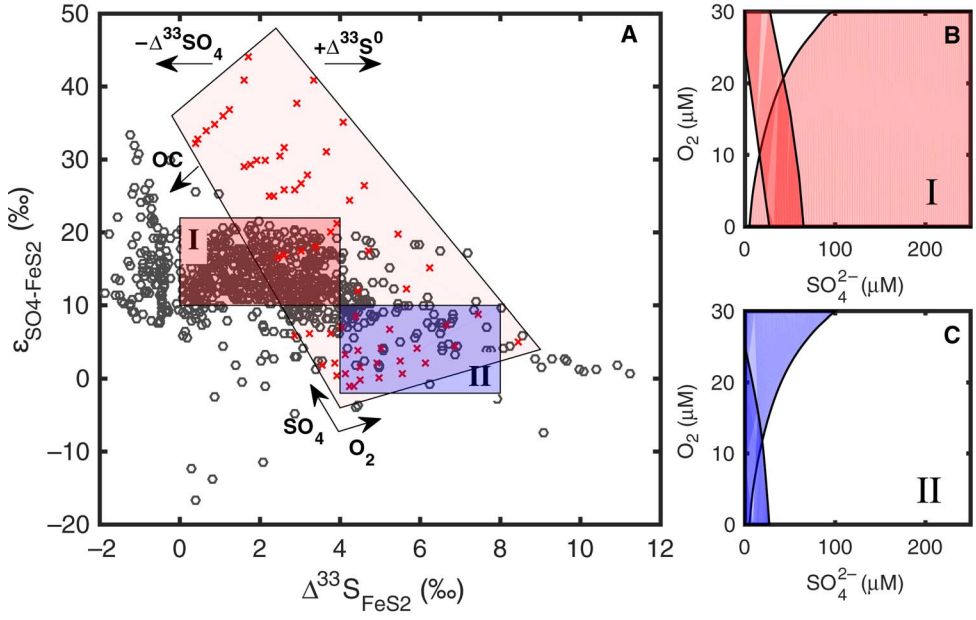

Fig. 3. Effect of oxygen, sulfate, organic matter, imposed $\Delta^{33}SO_4$, and $\Delta^{33}S^0$ on $\varepsilon_{SO4\text{-}FeS2}$ and $\Delta^{33}S_{FeS2}$. (**A**) Sulfur isotope data (circles) in Archean pyrites older than 2.4 Ga (*33*). Sulfate-pyrite isotopic differences $\varepsilon_{SO4\text{-}FeS2}$ were calculated from rock $\delta^{34}S$ values for the value of $\delta^{34}S$ in seawater sulfate of 12‰. Shaded region corresponds to the model's range in Fig. 2, obtained for sediment organic carbon (OC) content of 0.1%, the $\Delta^{33}S^0$ in the deposited elemental sulfur of 10‰, and the $\Delta^{33}SO_4$ in seawater sulfate of zero. Arrows indicate the directions in which the modeled range shifts in response to increases in indicated parameters. (**B** and **C**) Ranges (dark shading) of O_2 and sulfate that correspond to the isotopic ranges within the respective outlines I and II in (A). Lightly shaded areas correspond to the respective ranges in individual isotopic parameters, $\varepsilon_{SO4\text{-}FeS2}$ and $\Delta^{33}S_{FeS2}$, calculated for the same set of parameters as in Fig. 2. The modeled trends indicate that the preservation of large $\varepsilon_{SO4\text{-}FeS2}$ values observed after 2.7 Ga (Fig. 1) requires high sulfate, whereas the preservation of large $\Delta^{33}S_{FeS2}$ values requires the presence of O_2.

The reaction network R_{ij} for chemical species C_i considered sulfate reduction, reoxidation of the produced hydrogen sulfide, precipitation of iron monosulfide and subsequent formation of pyrite, and, variably, disproportionation of elemental S (fig. S1). Vertical transport in the sediment matrix of porosity φ was characterized by molecular diffusion coefficients D_i and burial velocity v neglected for solutes. A complete description of the model is given in the Supplementary Materials; the reactions and their rate formulations are listed in tables S1 and S2, and model parameter values are listed in table S3. The rate of sulfate reduction, a microbially mediated reaction known to impart the largest S isotopic fractionations, was simulated using Michaelis-Menten kinetics (table S2). The corresponding half-saturation concentration of sulfate, K_m, was on the order of low micromolar, consistent with values in modern low-sulfate environments (*13*), and the rate expression included a term that described inhibition of sulfate reduction in the presence of O_2. Isotopic fractionations during diagenetic reactions were calculated using specified fractionation factors (fig. S1). Patterns of the S isotope preservation were calculated for seawater sulfate concentrations between 1 and 400 μM and under a range of seawater O_2 concentrations between 0 and 30 μM. The effects of varied seawater O_2 and sulfate concentrations on pyrite $\delta^{34}S$ were expressed as deviations ($\varepsilon_{SO4\text{-}FeS2}$) relative to the value in sulfate from overlying water, which was set to 12‰ as the benchmark value for Archean seawater (*5*); alternative values are considered in the Supplementary Materials. To investigate the behavior of atmospherically derived MIF-S signals, our model assumed a flux of elemental S with a specified $\Delta^{33}S$ composition and predicted the fate of this MIF-S signal in sedimentary pyrite. Because the aerosol elemental S $\Delta^{33}S$ values were not likely to have been spatially uniform and the corresponding values of $\delta^{33}S$ and $\delta^{34}S$ in elemental S are not well constrained for the Archean, we set the isotopic composition of S^0 to $\Delta^{33}S_{S0}$ = 10‰ as a benchmark value (see Supplementary Materials) and varied this in a sensitivity analysis. Seawater sulfate was assumed to carry no MIF signal ($\Delta^{33}S_{SO4} = 0$) in benchmark simulations, but the model was also run for an alternative set of values ($\Delta^{33}S_{SO4} = -7$‰) (*9*). In comparison to previous models for the Archean S cycle (*4*, *8*), the present model expanded the range of modeled processes by including an oxidative cycle and elemental S disproportionation and by explicitly considering the kinetics of pyrite precipitation. Although timing the evolutionary appearance of microbial disproportionation is debated (*29*), we included it in the model to test for its possibility (*4*, *30*, *31*) and then verified that its absence does not modify our main conclusions. Similar to previous models (*4*, *8*), our model did not consider sulfate reduction coupled to anaerobic methane oxidation because its contribution to sulfate reduction in the Neoarchean was likely low given the slow kinetics of anaerobic methane oxidation at low sulfate concentrations, as observed in modern low-sulfate lakes (*8*, *32*). Furthermore, the corresponding S isotopic fractionations during methane oxidation are poorly known, confounding their description in our model (*32*).

SUPPLEMENTARY MATERIALS

Supplementary material for this article is available at http://advances.sciencemag.org/cgi/content/full/4/1/e1701835/DC1

section S1. Geochemical model
section S2. Isotopic model
section S3. Sensitivity analysis
table S1. Reactions included in the model.
table S2. Kinetics of the reactions included in the model.
table S3. Parameters for reactive transport modeling and sensitivity analysis.
table S4. Thermodynamic favorability of reactions suggested for elemental sulfur formation.
table S5. Model boundary conditions for sulfate, sulfide, and oxygen.
fig. S1. Sediment sulfur cycle with isotopic fractionation associated with each reaction.
fig. S2. Typical sediment profiles of sulfate, sulfide, oxygen, iron, CRS pool including FeS and elemental sulfur, and rates of reduction (R_{SR}) and reoxidation (R_{SOX}) along with isotopic fractionation of sulfate, sulfide, and pyrite for Archean conditions.
fig. S3. Change in $\varepsilon_{SO4\text{-}FeS}$ (‰) in response to changes in model parameter values.
fig. S4. Sensitivity of model outputs to organic matter availability at $[O_2]$ = 1 μM.
fig. S5. Sensitivity of model outputs to organic matter availability at $[SO_4]$ = 10 μM.
fig. S6. Effect of oxygen inhibition constant (K_i) on $\varepsilon_{SO4\text{-}FeS}$ at $[SO_4]$ = 10 μM.
fig. S7. Modeled range of $\Delta^{33}S_{FeS2}$ for which the atmospheric MIF-S signal is preserved in sedimentary pyrites, as a function of seawater oxygen and sulfate levels.
fig. S8. Effect of sulfate concentration on $\Delta^{33}S_{FeS2}$ at $[O_2]$ = 10 μM.
fig. S9. Effect of organic matter availability on $\Delta^{33}S_{FeS2}$ at $[SO_4]$ = 10 μM and $[O_2]$ = 10 μM.
fig. S10. Effect of oceanic oxygen level on $\Delta^{33}S_{FeS2}$ at $[SO_4]$ = 10 μM.
References (*34*–*58*)

REFERENCES AND NOTES

1. J. Farquhar, J. Savarino, S. Airieau, M. H. Thiemens, Observation of wavelength-sensitive mass-independent sulfur isotope effects during SO_2 photolysis: Implications for the early atmosphere. *J. Geophys. Res.* **106**, 32829–32839 (2001).
2. A. A. Pavlov, J. F. Kasting, Mass-independent fractionation of sulfur isotopes in Archean sediments: Strong evidence for an anoxic Archean atmosphere. *Astrobiology* **2**, 27–41 (2002).
3. H. Ohmoto, Y. Watanabe, H. Ikemi, S. R. Poulson, B. E. Taylor, Sulphur isotope evidence for an oxic Archaean atmosphere. *Nature* **442**, 908–911 (2006).
4. K. S. Habicht, M. Gade, B. Thamdrup, P. Berg, D. E. Canfield, Calibration of sulfate levels in the Archean ocean. *Science* **298**, 2372–2374 (2002).
5. D. E. Canfield, J. Farquhar, Animal evolution, bioturbation, and the sulfate concentration of the oceans. *Proc. Natl. Acad. Sci. U.S.A.* **106**, 8123–8127 (2009).
6. C. T. Reinhard, R. Raiswell, C. Scott, A. D. Anbar, T. W. Lyons, A late Archean sulfidic sea stimulated by early oxidative weathering of the continents. *Science* **326**, 713–716 (2009).
7. I. Halevy, D. T. Johnston, D. P. Schrag, Explaining the structure of the Archean mass-independent sulfur isotope record. *Science* **329**, 204–207 (2010).
8. S. A. Crowe, G. Paris, S. Katsev, C. Jones, S.-T. Kim, A. L. Zerkle, S. Nomosatryo, D. A. Fowle, J. F. Adkins, A. L. Sessions, J. Farquhar, D. E. Canfield, Sulfate was a trace constituent of Archean seawater. *Science* **346**, 735–739 (2014).
9. S. Ono, J. L. Eigenbrode, A. A. Pavlov, P. Kharecha, D. Rumble III, J. F. Kasting, K. H. Freeman, New insights into Archean sulfur cycle from mass-independent sulfur isotope records from the Hamersley Basin, Australia. *Earth Planet. Sci. Lett.* **213**, 15–30 (2003).
10. J. Farquhar, H. Bao, M. Thiemens, Atmospheric influence of Earth's earliest sulfur cycle. *Science* **289**, 756–758 (2000).
11. B. B. Jorgensen, A theoretical model of the stable sulfur isotope distribution in marine sediments. *Geochim. Cosmochim. Acta* **43**, 363–374 (1979).
12. M. B. Goldhaber, I. R. Kaplan, Mechanisms of sulfur incorporation and isotope fractionation during early diagenesis in sediments of the Gulf of California. *Mar. Chem.* **9**, 95–143 (1980).
13. M. Fakhraee, J. Li, S. Katsev, Significant role of organic sulfur in supporting sedimentary sulfate reduction in low-sulfate environments. *Geochim. Cosmochim. Acta* **213**, 502–516 (2017).
14. S. D. Domagal-Goldman, J. F. Kasting, D. T. Johnston, J. Farquhar, Organic haze, glaciations and multiple sulfur isotopes in the Mid-Archean Era. *Earth Planet. Sci. Lett.* **269**, 29–40 (2008).
15. K. Zahnle, M. Claire, D. Catling, The loss of mass-independent fractionation in sulfur due to a Palaeoproterozoic collapse of atmospheric methane. *Geobiology* **4**, 271–283 (2006).
16. I. Zhelezinskaia, A. J. Kaufman, J. Farquhar, J. Cliff, Large sulfur isotope fractionations associated with Neoarchean microbial sulfate reduction. *Science* **346**, 742–744 (2014).
17. M. Wille, J. D. Kramers, T. F. Nägler, N. J. Beukes, S. Schröder, T. Meisel, J. P. Lacassie, A. R. Voegelin, Evidence for a gradual rise of oxygen between 2.6 and 2.5 Ga from Mo isotopes and Re-PGE signatures in shales. *Geochim. Cosmochim. Acta* **71**, 2417–2435 (2007).
18. A. D. Czaja, C. M. Johnson, E. E. Roden, B. L. Beard, A. R. Voegelin, T. F. Nägler, N. J. Beukes, M. Wille, Evidence for free oxygen in the Neoarchean Ocean based on coupled iron–molybdenum isotope fractionation. *Geochim. Cosmochim. Acta* **86**, 118–137 (2012).
19. S. A. Crowe, L. N. Døssing, N. J. Beukes, M. Bau, S. J. Kruger, R. Frei, D. E. Canfield, Atmospheric oxygenation three billion years ago. *Nature* **501**, 535–538 (2013).
20. N. J. Planavsky, D. Asael, A. Hofman, C. T. Reinhard, S. V. Lalonde, A. Knudsen, X. Wang, F. O. Ossa, E. Pecoits, A. J. B. Smith, N. J. Beukes, A. Bekker, T. M. Johnson, K. O. Konhauser, T. W. Lyons, O. J. Rouxel, Evidence for oxygenic photosynthesis half a billion years before the Great Oxidation Event. *Nat. Geosci.* **7**, 283–286 (2014).

21. J. R. Waldbauer, D. K. Newman, R. E. Summons, Microaerobic steroid biosynthesis and the molecular fossil record of Archean life. *Proc. Natl. Acad. Sci. U.S.A.* **108**, 13409–13414 (2011).
22. X.-M. Liu, L. C. Kah, A. H. Knoll, H. Cui, A. J. Kaufman, A. Shahar, R. M. Hazen, Tracing Earth's O_2 evolution using Zn/Fe ratios in marine carbonates. *Geochem. Perspect. Lett.* **2**, 24–34 (2016).
23. N. Planavsky, A. Bekker, O. J. Rouxel, B. Kamber, A. Hofmann, A. Knudsen, T. W. Lyons, Rare earth element and yttrium compositions of Archean and Paleoproterozoic Fe formations revisited: New perspectives on the significance and mechanisms of deposition. *Geochim. Cosmochim. Acta* **74**, 6387–6405 (2010).
24. Q. Guo, H. Strauss, A. J. Kaufman, S. Schröder, J. Gutzmer, B. Wing, M. A. Baker, A. Bekker, Q. Jin, S.-T. Kim, J. Farquhar, Reconstructing Earth's surface oxidation across the Archean-Proterozoic transition. *Geology* **37**, 399–402 (2009).
25. A. Bekker, H. D. Holland, P.-L. Wang, D. Rumble III, H. J. Stein, J. L. Hannah, L. L. Coetzee, N. J. Beukes, Dating the rise of atmospheric oxygen. *Nature* **427**, 117–120 (2004).
26. J. F. Kasting, The rise of atmospheric oxygen. *Science* **293**, 819–820 (2001).
27. S. L. Olson, L. R. Kump, J. F. Kasting, Quantifying the areal extent and dissolved oxygen concentrations of Archean oxygen oases. *Chem. Geol.* **362**, 35–43 (2013).
28. J. F. Kasting, Models relating to Proterozoic atmospheric and oceanic chemistry, in *The Proterozoic Biosphere: A Multidisciplinary Study*, J. W. Schopf, C. Klein, Eds. (Cambridge Univ. Press, 1992), pp. 1185–1188.
29. D. T. Johnston, B. A. Wing, J. Farquhar, A. J. Kaufman, H. Strauss, T. W. Lyons, L. C. Kah, D. E. Canfield, Active microbial sulfur disproportionation in the Mesoproterozoic. *Science* **310**, 1477–1479 (2005).
30. P. Philippot, M. Van Zuilen, K. Lepot, C. Thomazo, J. Farquhar, M. J. Van Kranendonk, Early Archaean microorganisms preferred elemental sulfur, not sulfate. *Science* **317**, 1534–1537 (2007).
31. Y. Ueno, S. Ono, D. Rumble, S. Maruyama, Quadruple sulfur isotope analysis of ca. 3.5 Ga Dresser Formation: New evidence for microbial sulfate reduction in the early Archean. *Geochim. Cosmochim. Acta* **72**, 5675–5691 (2008).
32. K. Knittel, A. Boetius, Anaerobic oxidation of methane: Progress with an unknown process. *Annu. Rev. Microbiol.* **63**, 311–334 (2009).
33. D. T. Johnston, Multiple sulfur isotopes and the evolution of Earth's surface sulfur cycle. *Earth Sci. Rev.* **106**, 161–183 (2011).
34. R. A. Berner, *Early Diagenesis: A Theoretical Approach* (Princeton Univ. Press, 1980).
35. B. P. Boudreau, *Diagenetic Models and Their Implementation* (Springer, 1997).
36. K. Ingvorsen, B. B. Jørgensen, Kinetics of sulfate uptake by freshwater and marine species of *Desulfovibrio*. *Arch. Microbiol.* **139**, 61–66 (1984).
37. S. Katsev, S. A. Crowe, Organic carbon burial efficiencies in sediments: The power law of mineralization revisited. *Geology* **43**, 607–610 (2015).
38. J. Li, S. A. Crowe, D. Miklesh, M. Kistner, D. E. Canfield, S. Katsev, Carbon mineralization and oxygen dynamics in sediments with deep oxygen penetration, Lake Superior. *Limnol. Oceanogr.* **57**, 1634–1650 (2012).
39. D. E. Canfield, Factors influencing organic carbon preservation in marine sediments. *Chem. Geol.* **114**, 315–329 (1994).
40. D. J. Burdige, Preservation of organic matter in marine sediments: Controls, mechanisms, and an imbalance in sediment organic carbon budgets? *Chem. Rev.* **107**, 467–485 (2007).
41. D. E. Canfield, M. T. Rosing, C. Bjerrum, Early anaerobic metabolisms. *Philos. Trans. R. Soc. Lond. B Biol. Sci.* **361**, 1819–1834 (2006).
42. J. Li, thesis, University of Minnesota (2014).
43. D. E. Canfield, A. Teske, Late Proterozoic rise in atmospheric oxygen concentration inferred from phylogenetic and sulphur-isotope studies. *Nature* **382**, 127–132 (1996).
44. D. E. Canfield, B. Thamdrup, The production of 34S-depleted sulfide during bacterial disproportionation of elemental sulfur. *Science* **266**, 1973–1975 (1994).
45. D. E. Canfield, E. Kristensen, B. Thamdrup, *Aquatic Geomicrobiology* (Gulf Professional Publishing, 2005).
46. N. Pfennig, The phototrophic bacteria and their role in the sulfur cycle. *Plant Soil* **43**, 1–16 (1975).
47. D. E. Canfield, Isotope fractionation by natural populations of sulfate-reducing bacteria. *Geochim. Cosmochim. Acta* **65**, 1117–1124 (2001).
48. K. S. Habicht, D. E. Canfield, J. Rethmeier, Sulfur isotope fractionation during bacterial reduction and disproportionation of thiosulfate and sulfite. *Geochim. Cosmochim. Acta* **62**, 2585–2595 (1998).
49. A. S. Bradley, W. D. Leavitt, M. Schmidt, A. H. Knoll, P. R. Girguis, D. T. Johnston, Patterns of sulfur isotope fractionation during microbial sulfate reduction. *Geobiology* **14**, 91–101 (2016).
50. J. Farquhar, B. A. Wing, Multiple sulfur isotopes and the evolution of the atmosphere. *Earth Planet. Sci. Lett.* **213**, 1–13 (2003).
51. D. E. Canfield, Models of oxic respiration, denitrification and sulfate reduction in zones of coastal upwelling. *Geochim. Cosmochim. Acta* **70**, 5753–5765 (2006).
52. D. J. Burdige, A. Lerman, *Geochemistry of Marine Sediments* (Princeton Univ. Press, 2006).
53. P. Van Cappellen, Y. Wang, Cycling of iron and manganese in surface sediments: A general theory for the coupled transport and reaction of carbon, oxygen, nitrogen, sulfur, iron, and manganese. *Am. J. Sci.* **296**, 197–243 (1996).
54. S. Katsev, D. G. Rancourt, I. L'Heureux, dSED: A database tool for modeling sediment early diagenesis. *Comput. Geosci.* **30**, 959–967 (2004).
55. D. Dyrssen, K. Kremling, Increasing hydrogen sulfide concentration and trace metal behavior in the anoxic Baltic waters. *Mar. Chem.* **30**, 193–204 (1990).
56. P. Jourabchi, P. Van Cappellen, P. Regnier, Quantitative interpretation of pH distributions in aquatic sediments: A reaction-transport modeling approach. *Am. J. Sci.* **305**, 919–956 (2005).
57. S. Katsev, G. Chaillou, B. Sundby, A. Mucci, Effects of progressive oxygen depletion on sediment diagenesis and fluxes: A model for the lower St. Lawrence River Estuary. *Limnol. Oceanogr.* **52**, 2555–2568 (2007).
58. S. Kempe, E. T. Degens, An early soda ocean? *Chem. Geol.* **53**, 95–108 (1985).

Acknowledgments: We thank C. Reinhard and an anonymous reviewer for comments that helped improve the manuscript. **Funding:** This work was partially supported by Natural Sciences and Engineering Research Council of Canada Discovery grant 0487 to S.A.C.
Author contributions: M.F. performed modeling, interpreted results, and contributed to writing the manuscript as a first author. S.A.C. contributed ideas, helped place results in the context of available data, and contributed to writing. S.K. supervised the project, interpreted results, and contributed to writing. **Competing interests:** The authors declare that they have no competing interests. **Data and materials availability:** All data needed to evaluate the conclusions in the paper are present in the paper and/or the Supplementary Materials. Additional data related to this paper may be requested from the authors.

Submitted 1 June 2017
Accepted 19 December 2017
Published 24 January 2018
10.1126/sciadv.1701835

Citation: M. Fakhraee, S. A. Crowe, S. Katsev, Sedimentary sulfur isotopes and Neoarchean ocean oxygenation. *Sci. Adv.* **4**, e1701835 (2018).

Sedimentary sulfur isotopes and Neoarchean ocean oxygenation

Mojtaba Fakhraee, Sean A. Crowe and Sergei Katsev

Sci Adv **4** (1), e1701835.
DOI: 10.1126/sciadv.1701835